VULoc: Accurate UWB Localization for Countless Targets without Synchronization

JING YANG, Tsinghua University, China
BAISHUN DONG, Tsinghua University, China
JILIANG WANG, Tsinghua University, China

Ultra-WideBand (UWB) localization has shown promising prospects in both academia and industry. However, accurate UWB localization for a large number of tags (i.e., targets) is still an open problem. Existing works usually require tedious time synchronization and labor-intensive calibrations. We present VULoc, an accurate UWB localization system with high scalability for an unlimited number of targets, which significantly reduces synchronization and calibration overhead. The key idea of VULoc is an accurate localization method based on passive reception without time synchronization. Specifically, we propose a novel *virtual*-Two Way Ranging (V-TWR) method to enable accurate localization for an unlimited number of tags. We theoretically analyze the performance of our method and show its superiority. We leverage redundant ranging packets among anchors with known positions to infer a range mapping for auto-calibration, which eliminates the ranging bias arising from the hardware and multipath issues. We finally design an anchor scheduling algorithm, which estimates reception quality for adaptive anchor selection to minimize the influence of NLOS. We implement VULoc with DW1000 chips and extensively evaluate its performance in various environments. The results show that VULoc can achieve accurate localization with a median error of 10.5 cm and 90% error of 15.7 cm, reducing the error of ATLAS (an open-source TDOA-based UWB localization system) by 57.6% while supporting countless targets with no synchronization and low calibration overhead.

CCS Concepts: • **Networks** → **Location based services**.

Additional Key Words and Phrases: UWB localization, High accuracy, Scalable, Auto-calibration, No synchronization

ACM Reference Format:
Jing Yang, BaiShun Dong, and Jiliang Wang. 2022. VULoc: Accurate UWB Localization for Countless Targets without Synchronization. *Proc. ACM Interact. Mob. Wearable Ubiquitous Technol.* 6, 3, Article 148 (September 2022), 25 pages. https://doi.org/10.1145/3550286

1 INTRODUCTION

The emergence of Ultra-WideBand (UWB) technology has shown great potential to provide high-accuracy positioning for the Internet of Things (IoT) thanks to its nanosecond-level time resolution. As a result, UWB attracts great attention from both academia [17, 25, 30, 52, 56, 61] and industry [5, 6, 13, 14]. There are plenty of UWB localization research works, like concurrent ranging [23, 31], sports analysis [30], etc. Meanwhile, a large number of commercial UWB localization systems have been designed and implemented, e.g., Qorvo [7], Ubisense [5], and Apple [14].

Existing UWB localization approaches, however, have two limitations. First, existing approaches cannot achieve high position accuracy and scalability simultaneously. In practice, a large number of applications require both accuracy and scalability, e.g., positioning for large-scale items in shopping mall or stadium, positioning

Authors' addresses: Jing Yang, Tsinghua University, Haidian Qu, Beijing Shi, China, jing-yan18@mails.tsinghua.edu.cn; BaiShun Dong, Tsinghua University, Haidian Qu, Beijing Shi, China, dbs18@mails.tsinghua.edu.cn; Jiliang Wang, Tsinghua University, Haidian Qu, Beijing Shi, China, jiliangwang@tsinghua.edu.cn.

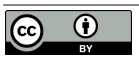

2474-9567/2022/9-ART148
https://doi.org/10.1145/3550286

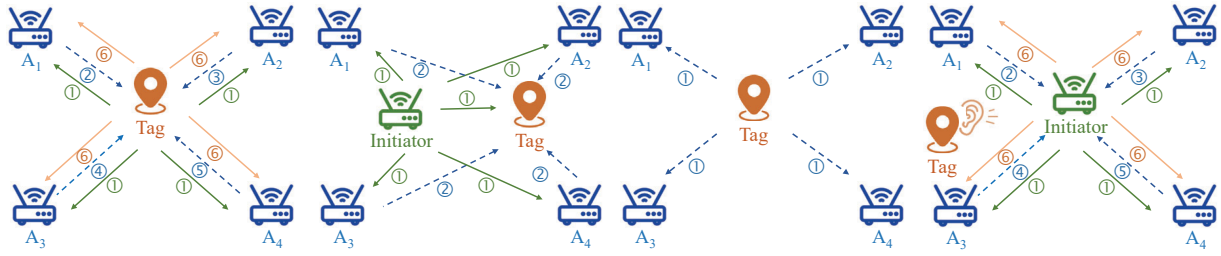

Fig. 1. UWB based localization schemes.

network for drone swarms that is sensitive to latency and collisions, and positioning a large group of robots for warehousing and logistics. Generally, there are mainly three localization schemes for UWB, namely, Two-way Ranging (TWR), Time Difference of Arrival (TDOA), and Angle of Arrival (AoA). The TWR scheme requires multiple message exchanges between the tag and anchors to calculate the Time of Flight (ToF) [34], as shown in Fig. 1a. We can locate the tag with different ToF to multiple anchors. As the number of tags increases, this leads to severe message collisions that hinder the scalability of the system. For the TDOA scheme in Fig. 1b, by recording timestamps of messages from anchors, a tag can calculate its position based on the time difference between different anchors. The scheme can scale to a large number of tags due to passively reception. However, it requires tight time synchronization between anchors. The clock drift among different anchors also introduces inevitable localization errors (see analysis in Sec 4.1). Thus, the accuracy of the TDOA scheme highly depends on the synchronization accuracy and is much lower than the TWR scheme. The AoA scheme, seen in Fig. 1c, is to estimate the angle between two devices and leverage angles to multiple anchors for localization [67, 69]. Though the number of message exchanges for a tag is small, it still incurs signal collisions as the number of tags increases. Furthermore, even a tiny angle error can cause a significant position error at a long distance. Therefore, there is an urgent demand for a UWB localization method that can simultaneously achieve high accuracy and scalability.

The second limitation is the inherent error for the estimated timestamp and range due to the defective hardware and environmental factors. We examine three main factors for ranging errors, i.e., the antenna delay, the clock drift of devices, and the rich multi-path in Sec. 2.2. To address ranging errors, existing UWB localization approaches usually try to calibrate through tedious manual efforts. For instance, they select multiple known locations in a specific environment to perform ranging calibration. They combine the estimated range and the actual range at those localizations for calibration. However, such methods are highly labor-intensive and environment-dependent, which significantly increases the application overhead. Moreover, the None-Line-Of-Sight (NLOS) effect further incurs ranging errors and degrades the performance of UWB localization, which cannot be solved simply by calibration.

We present VULoc, a novel UWB-based localization system to provide high accuracy and scalability simultaneously that significantly reduces time synchronization and calibration overhead. Fig. 1d shows the framework of VULoc. The key of VULoc is a novel virtual-TWR (V-TWR) scheme to enable accurate tag localization by passively overhearing. In VULoc, an anchor (namely *initiator*) initiates data transmissions. We design a message exchange scheme among the *initiator* and other anchors (A_i $i = 1, 2, \ldots, N$). A tag only overhears the messages and records the message timestamps during the entire process for localization. VULoc is composed of the following three components:

Virtual two-way ranging. The virtual two-way range (V-TWR) scheme enables accurate tag localization by passive receptions without time synchronization. Intuitively, we can apply TDOA localization after receiving packets from different anchors. However, TDOA localization requires accurate time synchronization among anchors. Instead of directly calculating the time difference between different anchors, VULoc takes advantage of the message exchange between the *initiator* and anchors. By overhearing those messages, VULoc derives a "virtual response" from the tag to the *initiator*, forming a virtual TWR process. VULoc infers the accurate timestamp of the "virtual response" by leveraging the positional geometric relationship of the tag and anchors. Therefore, VULoc can calculate the tag position based on those timestamps in the virtual TWR process. We theoretically prove that VULoc can provide accurate localization comparable to the original TWR method, even with clock drift among different anchors. As a result, VULoc can achieve high localization accuracy and support countless targets.

Range auto-calibration. There usually exist errors between the estimated range and the actual range due to the impact of the antenna delay, the clock drift of devices, and the multipath effect. We propose an anchor-assisted calibration method to resolve the problem instead of resorting to tedious manual calibrations. The insight is that the positions of anchors in UWB localization are usually known in advance. Meanwhile, thanks to the framework of VULoc, we can estimate ranges between the *initiator* and other anchors $A_i(i = 1, 2, \ldots, N)$ based on the exchanging messages among them. Therefore, we can infer the calibration model between the estimated and actual ranges for calibration. We show the feasibility of the anchor-assisted calibration model in Sec. 2.2. As a result, VULoc can achieve auto-calibration for various environments without manual efforts.

Anchor scheduling against None-Line-of-Sight (NLOS). Similar to other wireless systems, a major shortage of UWB localization is the impact of NLOS. For example, when the *initiator* is blocked by obstacles (e.g., the human body), the performance of the system significantly degrades. A straightforward method to avoid NLOS is to perform a round-robin scheduling for anchors, i.e., each anchor initiates the ranging process in turn to play the role of the *initiator*. However, such a method is still impacted by NLOS in some rounds. We propose a method to estimate reception quality for adaptive anchor selection to minimize the NLOS effect. Specifically, we first perform the round-robin scheduling for anchors. Then, we extract channel features based on each reception in each round for quality estimation. A higher quality indicates a more reliable recorded timestamp. We thus propose a metric to quantify the measurement quality in each round. Therefore, we can select the most reliable ranging results in each round for localization to minimize the NLOS effect.

Implementation and Evaluation. We implement VULoc on off-the-shelf DW1000 transceivers and conduct extensive experiments to show the localization and tracking performance of VULoc under various environments. We also show the performance of VULoc in different areas (80 m^2 *VS* 7200 m^2). We compare the performance of VULoc with the TWR method (i.e., DS-TWR) and an open-source TDOA-based method (i.e., ATLAS [62]) in a large-scale deployment of 30 nodes.

Main Results and Contributions.

- We present VULoc, a robust UWB-based localization system that achieves high accuracy and scalability to support countless tags.
- We propose a novel virtual two-way ranging (V-TWR) scheme to derive accurate tag position by passive receptions without time synchronization. We theoretically show that V-TWR achieves a high localization accuracy comparable to the original TWR method.
- We present an auto-calibration method by deriving an anchor-assisted model between estimated ranges and actual ranges of anchors.
- We implement VULoc on the commercial DW1000 chip and extensively evaluate its performance. The evaluation results show that VULoc can achieve a median error of 10.5 cm and a 90% error of 15.7 cm in various environments, improving the accuracy of ATLAS [62] by 57.6%. We also show that VULoc

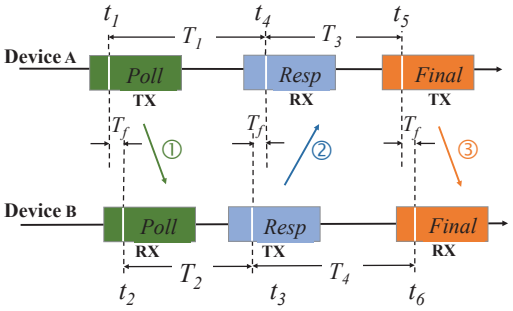

Fig. 2. The TWR process that involves three packets exchanges.

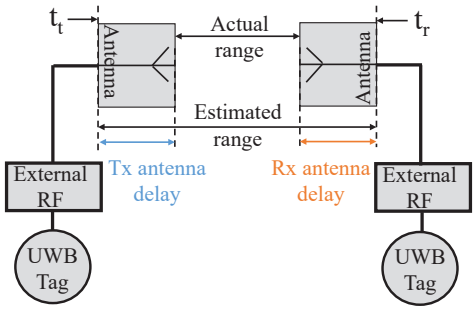

Fig. 3. The effect of antenna delay on ranging.

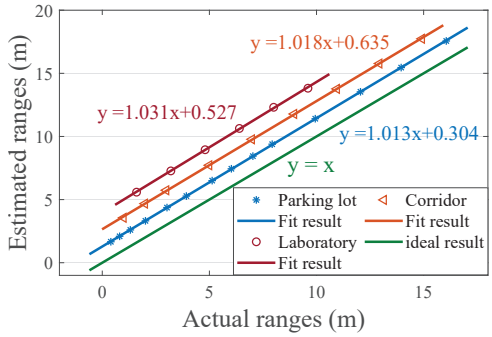

Fig. 4. Ranging result in various environments.

performs well even in a large area of 7200 m^2 and reduces 69.6% error on average compared to DS-TWR in a large-scale deployment of 30 nodes.

2 BACKGROUND

2.1 UWB Basics

Upon receiving a UWB message, a UWB receiver can estimate a nanosecond channel impulse response (CIR) thanks to its high bandwidth. CIR is a good description of the attenuation and delay of the received signal through the wireless channel. Given the transmitting signal $T(t)$, the receiving signal $R(t)$ and the CIR $H(t)$, we have [64]:

$$T(t) = R(t) * H(t) \tag{1}$$

where $H(t) = \sum_{i=1}^{L} \alpha_i e^{-j2\pi f_c \tau_i} \delta(t - \tau_i)$. L is the number of paths, τ_i and α_i are the delay and amplitude attenuation of the signal from path i, and $\delta(t - \tau_i)$ is the Dirac's delta function [9].

A typical CIR is shown in Fig. 5a. Each peak in the figure indicates a dominating transmission path. Actually, every point in the CIR is the superposition of the signals of several transmission paths. The UWB receiver estimates the first path of the CIR and adopts the corresponding time as the receiving timestamp. Fig. 5a shows an example first path (*FP*) estimated by the DW1000 chip [2]. In this way, we can obtain the timestamp of the receiving packet based on the timestamp of *FP*, and then use the timestamp for ranging.

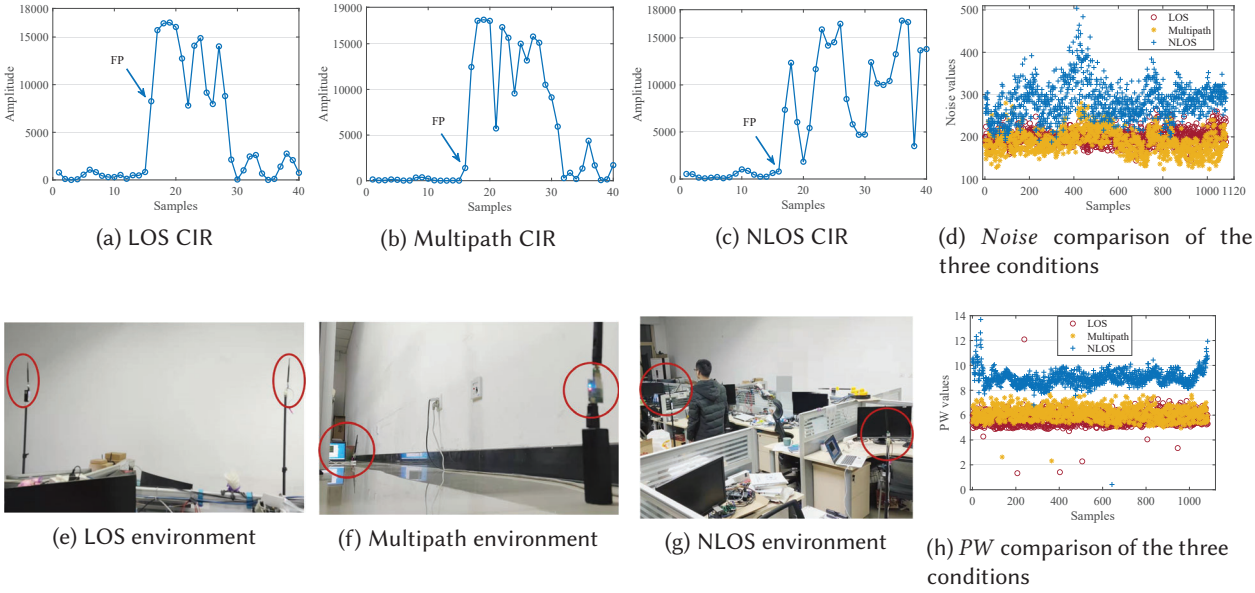

(a) LOS CIR (b) Multipath CIR (c) NLOS CIR (d) *Noise* comparison of the three conditions

(e) LOS environment (f) Multipath environment (g) NLOS environment (h) *PW* comparison of the three conditions

Fig. 5. Quality of receptions under the condition of LOS, multipath and NLOS. We adopt the *Noise* and *PW* metrics to show the reception quality.

2.2 Factors to Ranging Accuracy

Double-Sided Two Way Ranging (DS-TWR) is a widely used ranging method in UWB, which involves three packet exchanges, as illustrated in Fig. 2. With recorded timestamps, we can calculate the ToF between two devices:

$$\begin{aligned} T_f &= \frac{(t_4 - t_1) \times (t_6 - t_3) - (t_5 - t_4) \times (t_3 - t_2)}{(t_5 - t_1) + (t_6 - t_2)} \\ &= \frac{T_1 \times T_4 - T_3 \times T_2}{T_1 + T_3 + T_2 + T_4} \end{aligned} \tag{2}$$

Based on T_f, the range can be calculated as $T_f \times c$.

Though the DS-TWR method can achieve high-ranging accuracy localization, the estimated range is subject to many factors. We introduce three main factors, i.e., the antenna delay, the clock drift, and the multipath.

2.2.1 Antenna Delay. As shown in Fig. 3, when a UWB device receives a packet, it will record a timestamp (t_r) including the antenna delay (*Rx antenna delay*). As a result, the estimated range is equal to the sum of the actual range and an extra range due to antenna delays.

Without loss of generality, we assume the *Tx antenna delay* is t_a and the *Rx antenna delay* is t_b. Given a Tx timestamp t_t, we can calculate the actual Tx timestamp as $\widehat{t_t} = t_t + t_a$. Similarly, we can calculate the actual Rx timestamp as $\widehat{t_r} = t_r - t_b$, where t_r is the Rx timestamp. Thus we can calculate the time interval in Fig. 2 as:

$$\widehat{T_1} = T_1 - t_a - t_b;\ \widehat{T_3} = T_3 + t_a + t_b;\ \widehat{T_2} = T_2 + t_a + t_b;\ \widehat{T_4} = T_4 - t_a - t_b; \tag{3}$$

Substituting the equation into the Equ. (2), we have:

$$\begin{aligned}\widehat{T_f} =& \frac{(T_1 - t_a - t_b) \times (T_4 - t_a - t_b) - (T_3 + t_a + t_b) \times (T_2 + t_a + t_b)}{(T_1 - t_a - t_b) + (T_3 + t_a + t_b) + (T_2 + t_a + t_b) + (T_4 - t_a - t_b)} \\ =& \frac{T_1 \times T_4 - T_3 \times T_2}{T_1 + T_3 + T_2 + T_4} - (t_a + t_b) \\ =& T_f - (t_a + t_b)\end{aligned} \tag{4}$$

We can see that the antenna delay brings a constant deviation (i.e., $t_a + t_b$) to the range estimation.

2.2.2 Clock Drift. We now show the impact of the clock drift of devices on the ranging result. We assume the clock drift of device A as e_A and that of device B as e_B. We can model the time in Fig. 2 as:

$$\widehat{t_i} = (1 + e_A)t_i \ (i = 1, 4, 5); \quad \widehat{t_j} = (1 + e_B)t_j \ (j = 2, 3, 6); \tag{5}$$

And the time interval can be rewritten as:

$$\widehat{T_1} = (1 + e_A)T_1; \quad \widehat{T_3} = (1 + e_A)T_3; \quad \widehat{T_2} = (1 + e_B)T_2; \quad \widehat{T_4} = (1 + e_B)T_4; \tag{6}$$

As $T_1 + T_3 = T_2 + T_4$ ([66] [54]), the estimated range is:

$$\begin{aligned}\widehat{T_f} =& \frac{(1 + e_A)T_1 \times (1 + e_B)T_4 - (1 + e_B)T_2 \times (1 + e_A)T_3}{2 \times ((1 + e_A)T_1 + (1 + e_A)T_3)} \\ =& (1 + e_B)T_f\end{aligned} \tag{7}$$

2.2.3 Multipath. Based on the above derivation results, we know the estimated range and the actual range should show a roughly linear relationship. Thus, we conduct ranging experiments in various environments to verify the claim. We use a pair of UWB nodes and adopt the DS-TWR method for ranging, and we collect data for about 30 seconds and calculate the average result as the estimated range for each position. Fig. 4 shows the result.

We show the results in various environments, including a parking lot, a laboratory, and a corridor. We fit those points and can see a linear relationship between the estimated ranges and the actual ranges within 20 meters. We also notice that the relationship varies in different environments. For instance, there is around a 0.3m deviation between the parking lot and the corridor. We think this phenomenon is caused by multipath. The multipath effect can lead to biased timestamps and thus range errors. As a result, the ranging result can vary significantly in different environments.

2.3 Quality of Reception

UWB offers rich and fine-grained information about the communication channel that can be used to estimate the quality of receptions. The higher reception quality indicates a more reliable recorded timestamp. To estimate the quality of receptions, we adopt two metrics, namely *Noise* and *PW* [4]. *Noise* is the standard deviation of CIR Noise values. *PW* is the difference between *RX_POWER* and *FP_POWER*, where *RX_POWER* is the total power of the receiving signal and *FP_POWER* is only the power of the first path signal. Intuitively, *PW* indicates the ratio of the energy of the first path to that of all paths. Both *Noise* and *PW* metrics can be calculated from the CIR.

We compare UWB receptions in three conditions, i.e., LOS, rich multipath, and NLOS, to investigate the variation of the reception quality. Fig. 5e to Fig. 5g show the deployment in the three environments, with the corresponding CIR shown in Fig. 5a to Fig. 5c. We can see that the first path is sharp and can be easily differentiated from other paths in the LOS and multipath conditions. Besides, the accumulated power for the first path is typically the major part of the entire CIR [4]. In NLOS conditions, however, the first path amplitude becomes much weaker, and the accumulated power of the first path drops sharply. We then calculate the *Noise*

and *PW* metrics in these conditions and show the comparison in Fig. 5d and Fig. 5h. We see that the NLOS values are larger than LOS and multipath values no matter the *Noise* or *PW* metric. Meanwhile, the LOS values and the multipath values are nearly the same. We can draw two conclusions from the experiment, 1) the *Noise* and *PW* metrics can effectively distinguish the reception quality in LOS and NLOS conditions. The high values of two metrics indicate a poor reception quality, and 2) we show UWB is resistant to multipath as indicators in multipath and LOS conditions are basically consistent.

3 SYSTEM DESIGN

Fig. 1d shows the framework of VULoc with five anchors. An anchor (namely *initiator*) initiates data transmissions. The corresponding data flow of VULoc is shown in Fig. 6. VULoc exchanges messages between the *initiator* and other anchors and lets the tag keep passively receiving. For each pair of the *initiator* and an anchor, VULoc records a total of six timestamps, forming the TWR process shown in Fig. 2. As a result, we can calculate the range between the *initiator* and other anchors by Equ. (2). Meanwhile, the tag passively overhears six packets. Upon receiving a packet, we can estimate the corresponding timestamp and calculate two channel metrics, i.e., *Noise* and *PW*, which indicate the reception quality. We show how VULoc can achieve high accuracy and scalability with the following three components, i.e., the virtual two-way ranging (V-TWR) scheme, the range auto-calibration method, and the anchor scheduling algorithm.

3.1 Virtual Two-way Ranging (V-TWR) Scheme

In VULoc, each pair of the *initiator* and an anchor forms a $Poll - Resp - Final$ data exchange as stated by the DS-TWR method. We denote t_{IP} and t_{IF} as the sending time for the *Poll* and *Final* packet, t_{IRi} as the receiving time for the *Resp* packet from the ith anchor. Similarly, we denote t_{TP} and t_{TF} as the receiving time of the *Poll* and *Final* packet, t_{TRi} as the receiving time for the *Resp* packet of ith anchor, $i = 1, \ldots, N$ where N is the number of anchors. Fig. 6 shows an example of marked timestamps with the *initiator* and the other four anchors. Note that in the *Final* packet, the *initiator* adds all recorded timestamps in the packet payload. Therefore, the tag can obtain 12 timestamps in total for each round. The target of V-TWR is designed to use those 12 timestamps for tag localization.

With those timestamps, the classic approach is the so-called TDOA [43, 62]. However, such a method requires tight time synchronization among anchors to achieve satisfactory positioning accuracy. Time synchronization is still an open issue without a perfect solution, causing much lower accuracy than that of the TWR method. We theoretically show in Sec. 4.1 that the TDOA method can lead to more localization errors, an order of magnitude larger than VULoc, due to clock drift among different anchors.

3.1.1 Virtual Response Generation. Instead of using the classic TDOA method, VULoc takes advantage of the redundant data exchanged between the *initiator* and other anchors. The intuitive idea is to leverage the message exchange to derive the range.

The novel idea of VULoc is to generate a *virtual response* from the tag for the *Poll* packet of the *initiator*. Then the tag and the *initiator* can form the $Poll - Resp - Final$ packet exchanges as that in the DS-TWR method. We take one anchor as an example and illustrate the process in Fig. 7. We generate a virtual *Resp* packet from the tag (transmitting at time t'_{TR1}) to the *initiator*, and assume the *virtual Resp* packet is received by the *initiator* at exact time t_{IR1}. Thus we can form a virtual TWR process between them and calculate the *initiator*-tag range by the Equ. (2):

$$T_f = \frac{(t_{IR1} - t_{IP}) \times (t_{TF} - t'_{TR1}) - (t'_{TR1} - t_{TP}) \times (t_{IF} - t_{IR1})}{t_{IF} - t_{IP} + t_{TF} - t_{TP}} \tag{8}$$

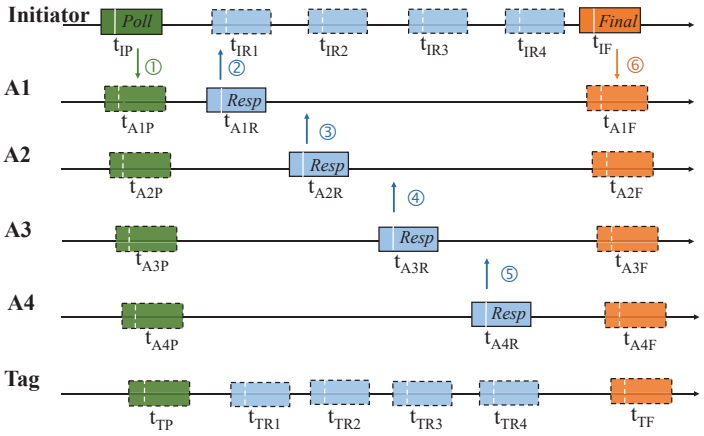

Fig. 6. The data flow of VULoc with five anchors. An anchor (namely *initiator*) initiates data transmissions.

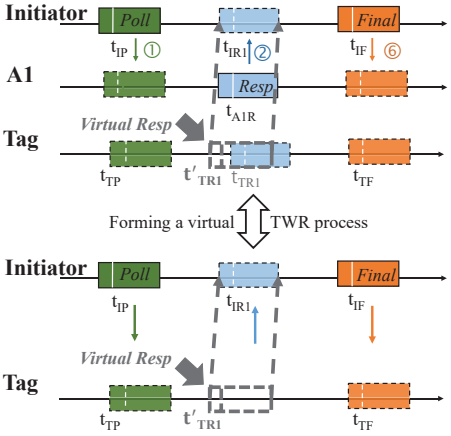

Fig. 7. Virtual responses generation process with an anchor.

T_f cannot be directly calculated due to the unknown t'_{TR1}, and thus we call it the *virtual* range. In order to calculate the range, we should derive the transmitting time t'_{TR1} for the *virtual Resp* packet. We leverage the position relationship between the three UWB devices to resolve the problem. Denote the range between the tag and the *initiator* as $d_{T\to I}$, the range between the *initiator* and the anchor A_1 as $d_{I\to A_1}$, and the range between the tag and the anchor as $d_{T\to A1}$, we can calculate the time t_{IR1}, t_{TR1} and t'_{TR1} as:

$$t_{TR1} = t_{A1R} + \frac{d_{T\to A}}{c} \tag{9a}$$

$$t_{IR1} = t_{A1R} + \frac{d_{I\to A}}{c} \tag{9b}$$

$$t_{IR1} = t'_{TR1} + \frac{d_{T\to I}}{c} \tag{9c}$$

where c is the light speed. Based on the above equations, we can derive t'_{TR1} as:

$$t'_{TR1} = t_{TR1} - \frac{d_{T\to A}}{c} - \frac{d_{T\to I}}{c} + \frac{d_{I\to A}}{c} \tag{10}$$

Combine Equ. (10) and Equ. (8), we can eliminate t'_{TR1} and obtain the following equation:

$$\frac{d_{T\to I}}{c} \times CT = \frac{d_{T\to A} + d_{T\to I} - d_{I\to A}}{c} \times (t_{IF} - t_{IP}) + C_{x1} \tag{11}$$

where CT and $Cx1$ are calculated as follows:

$$\begin{aligned} CT &= (t_{IF} - t_{IP}) + (t_{TF} - t_{TP}) \\ C_{x1} &= (t_{IR1} - t_{IP}) \times (t_{TF} - t_{TR1}) \\ &\quad - (t_{TR1} - t_{TP}) \times (t_{IF} - t_{IR1}) \end{aligned} \tag{12}$$

We observe that CT is a constant for the same pair of the *initiator* and the tag (Fig. 6), while C_{x1} is specific for each anchor (e.g., C_{x1} for A_1). Due to two unknown parameters $d_{T\to I}$ and $d_{T\to A}$ in the above equations, we cannot calculate the tag's position. However, we obtain a relationship between the $d_{T\to I}$ and $d_{T\to A}$. In the next section, we show how VULoc resolves the tag position with the relationship.

3.1.2 Virtual Time Recovery. VULoc proposes a novel insight that the distance $d_{T\to I}$ (tag-*initiator*) remains the same concerning different anchors since the whole process in Fig. 6 is very fast (on the order of several milliseconds). We thus can assume that the distance between the *initiator* and the tag has not changed. Hence, VULoc uses the collaboration of multi-anchors to resolve the problem.

For anchors 1 to 4, we can re-organize Equ. (11) and (12) as follows ($i = 1 \ldots 4$):

$$\frac{d_{T\to I}}{c} \times CT = \frac{d_{T\to Ai} + d_{T\to I} - d_{I\to Ai}}{c} \times (t_{IF} - t_{IP}) + C_{xi} \tag{13}$$

where CT is a constant as shown in the above equations, and C_{xi} is calculated as:

$$\begin{aligned} C_{xi} = (t_{IRi} - t_{IP}) \times (t_{TF} - t_{TRi}) \\ - (t_{TRi} - t_{TP}) \times (t_{IF} - t_{IRi}) \end{aligned} \tag{14}$$

By subtracting the equations of anchor A_2 and A_1, we can infer the following equation:

$$\frac{d_{T\to A2} - d_{T\to A1}}{c} = \frac{(C_{x1} - C_{x2})}{t_{IF} - t_{IP}} + \frac{d_{I\to A2} - d_{I\to A1}}{c} \tag{15}$$

Note that $\frac{d_{T\to A2} - d_{T\to A1}}{c}$ in the left part of the Equ. (15) is the time difference from the tag to anchor $A2$ and $A1$. As all parameters in the right part of the equation are known, we can calculate the time difference from tag to $A2$ and $A1$ based on the recorded timestamps and known ranges between anchors.

Similarly, we can derive $\frac{d_{T\to A3} - d_{T\to A1}}{c}$ and $\frac{d_{T\to A4} - d_{T\to A1}}{c}$ for the anchor A_3 and A_4:

$$\frac{d_{T\to A3} - d_{T\to A1}}{c} = \frac{(C_{x1} - C_{x3})}{t_{IF} - t_{IP}} + \frac{d_{I\to A3} - d_{I\to A1}}{c} \tag{16}$$

$$\frac{d_{T\to A4} - d_{T\to A1}}{c} = \frac{(C_{x1} - C_{x4})}{t_{IF} - t_{IP}} + \frac{d_{I\to A4} - d_{I\to A1}}{c} \tag{17}$$

We now can use the time differences (i.e., Equ. (15) (16) (17)) from the tag to different anchors to locate the tag.

3.1.3 Localization with Virtual Timestamps. We investigate two widely used algorithms to resolve the tag position, i.e., the hyperbola-based algorithm and the search-based non-linear least square algorithm.

The hyperbola-based algorithm tries to derive the position directly based on hyperbolic equations. Theoretically, the tag is on a hyperbola with those fixed anchors as the focal points. Thus, we can calculate the position as the intersection point of different hyperbolas. Specifically, in VULoc, we adopt the widely used Chan algorithm [20]. The Chan algorithm assumes Gaussian noise with zero mean and solves the hyperbolic equations non-recursively. Thus, it has the advantage of requiring less computation.

Another widely used algorithm is the search-based non-linear least squares algorithm. Specifically, given a candidate position p_1 from solution space and anchors' positions p_{ai} ($i = 1, 2, 3 \ldots, N$ where N is the number of anchors), we can estimate the time difference of two anchors:

$$\Delta d_{i,j} = ||p_1 - p_{ai}|| - \left\|p_1 - p_{aj}\right\| \ , i \neq j \tag{18}$$

Since we have measured $\Delta\widehat{d}_{i,j}$, we can calculate the tag position by minimizing the difference between the estimated and measured values:

$$\widehat{p}_1 = \arg\min_{p} \textstyle\sum_{i=1}^{N-1} (\Delta\widehat{d}_{i,j} - \Delta d_{i,j})^2 \tag{19}$$

The algorithm usually searches in the entire space and thus is time-consuming yet very accurate.

The hyperbola-based algorithm provides a coarse position estimation with a low overhead. The search-based non-linear least square algorithm can provide a fine-grained result but with a high overhead incurred from space search. Thus, VULoc combines those two algorithms to trade off the accuracy and the time overhead. Specifically, VULoc first leverages the hyperbola-based algorithm to derive a coarse location by solving the intersection of

hyperbolas. Then, VULoc search in the vicinity of the coarse location with search-based non-linear least squares algorithm to obtain the fine-grained result.

3.2 Range Auto-calibration

As shown in Sec. 2.2, we investigate three main factors that lead to a large deviation between the estimated range and actual range, including the antenna delay, clock drift, and multipath. As a result, we need to calibrate the range to reduce the influence of those factors in order to achieve accurate positioning.

The traditional calibration method is applied through tedious manual calibration in advance, which is very labor-intensive. For instance, to calibrate the antenna delay of UWB devices, we should place three UWB devices at fixed positions and use an optimized method to calculate the constant deviation between the estimated ranges and the actual ranges [55]. However, the multipath effect of different environments will lead to different deviation patterns on the ranging result, as shown in Sec 2.2. As a result, we need to recalibrate the results in different environments to achieve a satisfactory ranging result.

We show the linear relationship between the estimated range and the actual range under the impact of those factors. In this way, we can use the linear relationship to simplify the calibration process. However, it still requires labor-intensive calibration in advance to obtain the relationship. Thus, we propose an anchor-assisted calibration model to obtain the range mapping at a low cost.

Specifically, we observe that the positions of anchors are accurately preset and known in UWB localization systems. Thus, we can obtain the position of these anchors (the *initiator* is also an anchor of a particular role) and figure out the actual ranges between them. Meanwhile, VULoc can calculate the ranges between the *initiator* and other anchors by adopting the ranging algorithm. Then, we can fit those pairs of the estimated range and the actual range to derive a linear mapping, as shown in Fig. 4. Assume the calibrated parameters are K and B, and given the estimated range $\widehat{d}$, we can infer the actual range d as:

$$d = (\widehat{d} - B)/K \tag{20}$$

The equation reveals the mapping between the estimated range and the actual range, and we can use the mapping to calibrate ranging results. To cope with different environments, we can use online exchanging messages for specific anchors in that environment for calibration. Therefore, we can apply an auto-calibration method to adapt to various environments. Note that other UWB localization systems can also leverage our method for auto-calibration at the cost of an extra ranging process for anchors.

We now show how VULoc uses Equ (20) for calibration. Due to the deviation, we can rewrite the Equ. (9) as:

$$\begin{aligned} t_{TR1} =& t_{A1R} + (\frac{d_{T\to A}}{c} \times K + B) \\ t_{IR1} =& t_{A1R} + (\frac{d_{I\to A}}{c} \times K + B) \\ t_{IR1} =& t'_{TR1} + (\frac{d_{T\to I}}{c} \times K + B) \end{aligned} \tag{21}$$

We then repeat the derivation process from Equ. (8) to Equ. (13) and have:

$$(\frac{d_{T\to I}}{c} \times K + B) \times CT = \frac{(d_{T\to Ai} \times K + B) + (d_{T\to I} \times K + B) - (d_{I\to Ai} \times K + B)}{c} \times (t_{IF} - t_{IP}) + C_{xi} \tag{22}$$

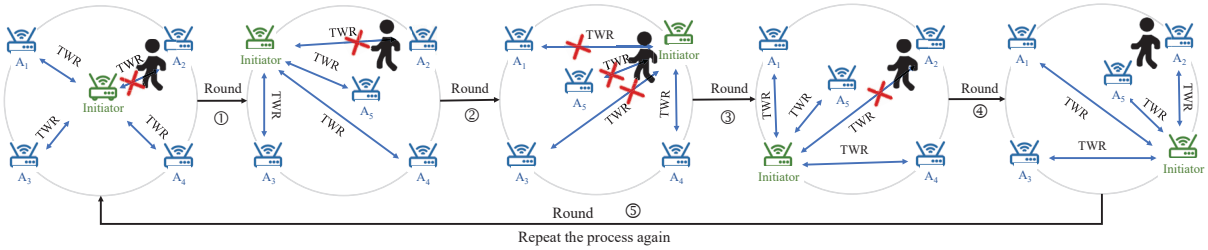

Fig. 8. The process of the anchor scheduling algorithm. Links of high quality are used for localization. NLOS links are avoid during the process.

After combining multiple anchors, we finally derive the calibrated results as:

$$\begin{aligned}
\frac{d_{T\to A2}-d_{T\to A1}}{c} &= \frac{(C_{x1}-C_{x2})}{(t_{IF}-t_{IP})K}+\frac{d_{I\to A2}-d_{I\to A1}}{c}\\
\frac{d_{T\to A3}-d_{T\to A1}}{c} &= \frac{(C_{x1}-C_{x3})}{(t_{IF}-t_{IP})K}+\frac{d_{I\to A3}-d_{I\to A1}}{c}\\
\frac{d_{T\to A4}-d_{T\to A1}}{c} &= \frac{(C_{x1}-C_{x4})}{(t_{IF}-t_{IP})K}+\frac{d_{I\to A4}-d_{I\to A1}}{c}
\end{aligned} \tag{23}$$

Then we can use the localization method in Sec. 3.1.3 to locate the tag with the calibrated results.

3.3 Anchor Scheduling Algorithm

Similar to other wireless localization systems, major errors can occur in the localization results of NLOS. Specially, we notice that VULoc is very sensitive to the selection of the *initiator* as the *initiator* needs to exchange data with other anchors. To minimize the NLOS effect, a straightforward round-robin scheduling method for anchors can be used to eliminate dependence on a specific anchor. Instead of applying a fixed anchor as the *initiator*, each anchor takes turns to be the *initiator*. Assuming there are five anchors, we let each anchor initiate transmissions in turns, e.g., based on their addresses. As shown in Fig. 8, we assume one of the links is blocked, e.g., by a person standing in the upper right corner. At the beginning of round 1, anchor A_1 becomes the *initiator* and performs the TWR process (Fig. 2) with the other four anchors. The two devices exchange three packets, i.e., *Poll*, *Resp*, and *Final*. The *initiator* embeds its address in each packet. After the *Final* packet, all anchors should parse the packet's source address (*src_addr*) and determine the next anchor to initiate the transmission. Based on the rule, A_2 will take turns to be the *initiator* and initiate the transmission. When round 5 is finished, VULoc will repeat the process. Furthermore, each anchor can back off with a time period proportional to its address upon receiving the *Final* packet. In such a way, even when one anchor does not work, its neighboring anchor can continue the scheduling process when its timer expires.

During the processing of the above scheduling, VULoc manages to estimate reception quality by extracting features of wireless channels for adaptive anchor selection to minimize the NLOS effect. For example, in round 2, three links are blocked by the human body, and we should avoid using those three links in localization. The idea is to estimate the quality of timestamps of each packet before using it for localization. Therefore, VULoc can select the appropriate links and timestamps for positioning. Specifically, we leverage two channel features, namely *Noise* and *PW*, to estimate the quality of receptions. As shown in Sec. 2.2, the value of both *Noise* and *PW* increases when links are blocked by obstacles like human beings. Thus, a higher value of *Noise* and *PW* indicates a lower quality of the message. However, the data flow of VULoc is more complicated, and we cannot directly use this to select the anchor. As shown in Fig. 7, the quality of receptions (Equ. 13) involves three devices,

the *initiator*, an anchor, and the tag. The tag has three receptions: the *Poll* and *Final* packets from the *initiator* and the *Resp* packets from the anchor. Thus, we should consider both the quality of reception from the *initiator* and from the anchor. To infer the quality of the measurement, we propose a confidence parameter cp that is calculated as:

$$cp = \frac{Noise_{poll}}{Noise_{max}} \times \frac{Noise_{Final}}{Noise_{max}} \times \frac{Noise_{Resp}}{Noise_{max}} \times 0.5 + \frac{PW_{poll}}{PW_{max}} \times \frac{PW_{Final}}{PW_{max}} \times \frac{PW_{Resp}}{PW_{max}} \times 0.5 \tag{24}$$

where $Noise_{max}$ and PW_{max} are empirical thresholds. The equation considers the reception quality of all three packets and normalizes the data by the maximum value of both metrics. We then assign the same weight (i.e., 0.5) to both metrics as we think they are equally important. We can adjust the weights according to the characteristics of the data. Based on the confidence parameter cp, we can select high quality message exchanges for localization. For example, we can filter out round 2 in Fig. 8 and discard the occluded links in every selected round, i.e., links that are blocked by human beings.

4 PERFORMANCE ANALYSIS

4.1 Localization Accuracy Comparison

We present a theoretical error analysis of our V-TWR scheme and show its superiority. For ease of understanding, we consider the uncalibrated case and start with the error analysis under the premise that the specific timestamp of the *virtual response* is known. As shown in Fig. 7, with the *virtual response* (t'_{TR1}), the tag and the *initiator* form the $Poll - Resp - Final$ packets exchange. We denote $T_1 = t_{IR1} - t_{IP}, T_2 = t'_{TR1} - t_{TP}, T_3 = t_{IF} - t_{IR1}, T_4 = t_{TF} - t'_{TR1}$, the ToF between devices is calculated by Equ. (2):

$$T_f = \frac{T_1 \times T_4 - T_2 \times T_3}{2 \times (T_1 + T_3)} \tag{25}$$

Denoting e_T and e_I as the clock drift of the tag and the *initiator*, we can model the time as:

$$\widehat{T_1} = (1 + e_I)T_1 \quad \widehat{T_2} = (1 + e_T)T_2 \tag{26a}$$

$$\widehat{T_3} = (1 + e_I)T_3 \quad \widehat{T_4} = (1 + e_T)T_4 \tag{26b}$$

Taking the clock drift into consideration, the estimated ToF $\widehat{T_f}$ can be calculated as [54] [66]:

$$\begin{aligned} \widehat{T_f} &= \frac{\widehat{T_1} \times \widehat{T_4} - \widehat{T_2} \times \widehat{T_3}}{2 \times (\widehat{T_1} + \widehat{T_3})} \\ &= (1 + e_I)T_f \end{aligned} \tag{27}$$

Therefore, the error is:

$$error = \widehat{T_f} - T_f = e_I T_f \tag{28}$$

Given the propagation time of 100 ns and a crystal clock of ± 20 ppm [4], we can calculate the value of error as $20e^{-6} * 100e^{-9} = 2ps$.

For VULoc, however, we cannot directly calculate the error following the above steps since the exact time of the *virtual response* is unknown. Without loss of generality, we focus on the estimated time difference from the tag to the anchor A_2 and A_1 (i.e., $\frac{d_{T\to A2} - d_{T\to A1}}{c}$) calculated by Equ. (15). We denote e_I, e_A and e_T as the clock drift of the *initiator*, the anchors, and the tag, respectively. Considering the clock drift, we can model the timestamps of devices (Fig. 6) as:

$$\widehat{t_{Ix}} = (1 + e_I)t_{Ix} \tag{29a}$$

$$\widehat{t_{Ax}} = (1 + e_A)t_{Ax} \tag{29b}$$

$$\widehat{t}_{Tx} = (1 + e_T)t_{Tx} \tag{29c}$$

where $x = P, R, F$.

Meanwhile, the difference between $\widehat{t}_{TR1}$ and $\widehat{t}_{A1R}$ is no longer a simple value $\frac{d_{T\to A}}{c}$ but the value multiplied by a coefficient $(1 + e_T)$ due to clock drift, i.e.,

$$\widehat{t}_{TR1} = \widehat{t}_{A1R} + \frac{d_{T\to A}}{c}(1 + e_T) \tag{30}$$

Similarly, we can rewrite the other two equations of Equ. (9) as:

$$\widehat{t}_{IR1} = \widehat{t}_{A1R} + \frac{d_{I\to A}}{c}(1 + e_I) \tag{31a}$$

$$\widehat{t}_{IR1} = \widehat{t}'_{TR1} + \frac{d_{T\to I}}{c}(1 + e_I) \tag{31b}$$

Combining these equations and eliminating the parameter $\widehat{t}_{A1R}$, we have:

$$\widehat{t}'_{TR1} = \widehat{t}_{TR1} - \frac{d_{T\to A}}{c}(1 + e_T) + \frac{d_{I\to A}}{c}(1 + e_I) - \frac{d_{T\to I}}{c}(1 + e_I) \tag{32}$$

With this equation, we again calculate $\frac{d_{T\to A2} - d_{T\to A1}}{c}$ following the process from Equ. (8) $\to$ (15) and have:

$$\frac{d_{T\to A2} - d_{T\to A1}}{c} = \frac{1}{1 + e_T}\left(\frac{\widehat{C}_{x1} - \widehat{C}_{x2}}{\widehat{t}_{IF} - \widehat{t}_{IP}} + \frac{d_{I\to A2} - d_{I\to A1}}{c}(1 + e_I)\right) \tag{33}$$

where $\widehat{C}_{xi}$ $(i = 1, 2)$ is calculated as follows:

$$\widehat{C}_{xi} = (\widehat{t}_{IRi} - \widehat{t}_{IP}) \times (\widehat{t}_{TF} - \widehat{t}_{TRi}) - (\widehat{t}_{TRi} - \widehat{t}_{TP}) \times (\widehat{t}_{IF} - \widehat{t}_{IRi}) \tag{34}$$

We can infer that $\frac{\widehat{C}_{x1} - \widehat{C}_{x2}}{\widehat{t}_{IF} - \widehat{t}_{IP}} = \frac{(1+e_I)(1+e_T)(C_{x1} - C_{x2})}{(1+e_I)(t_{IF} - t_{IP})} = (1 + e_T)(\frac{C_{x1} - C_{x2}}{t_{IF} - t_{IP}})$. Meanwhile, the estimated result of $\frac{d_{T\to A2} - d_{T\to A1}}{c}$ without considering clock drift is expressed in Equ. (15). Thus, the error due to the clock drift is calculated by the difference between Equ. (34) and Equ. (15):

$$error = \frac{d_{I\to A2} - d_{I\to A1}}{c} \times \frac{e_I - e_T}{1 + e_T} \tag{35}$$

Example. Given a distance difference of 30 m $(d_{I\to A2} - d_{I\to A1})$ and a clock drift of ± 20 ppm, we can calculate the error as $error = \frac{30}{3e^8} \times \frac{40e^{-6}}{(1+20e^{-6})} = 4\,ps$, which is comparable to that of the original TWR method (2 ps). The incurred range error is about $4e^{-12} \times 3 \times 10^8 m/s = 0.12\,cm$.

Error analysis for existing UWB localization approaches. Based on the recorded six timestamps from different anchors shown in Fig. 6, we can also perform the TDOA method for localization. We now analyze the error of TDOA-based methods and explain why VULoc is more accurate.

We assume that the error of the method is mainly induced by the clock drift of anchors, which is further proportional to the time interval $t_{AiR} - t_{AiP}$ $(i = 1, 2, 3, 4)$ (see Fig. 6). Given the clock drift of anchor A_i as e_i, the error of the TDOA method can be roughly estimated as:

$$error = (t_{AiR} - t_{AiP}) \times e_i - (t_{A1R} - t_{A1P}) \times e_1 \quad i > 1 \tag{36}$$

Typically, the value of $t_{Ai2} - t_{Ai1}$ $(i = 1, 2, 3, 4)$ is in the magnitude of thousands of microseconds [54, 66]. Given the clock drift of ±20 ppm of UWB devices and 100 μs time interval between two adjacent anchors (i.e., $(t_{AiR} - t_{AiP}) - (t_{A1R} - t_{A1P})$), the error can be calculated as $100e^{-6} \times 20e^{-6} = 2\,ns$, which translates into the distance error of 0.6 m. This is much larger than that of VULoc.

Note that this error analysis is a rough result of the TDOA method. As we all know, the positioning result is also highly dependent on the effect of time synchronization. As a result, the TDOA method can achieve a much

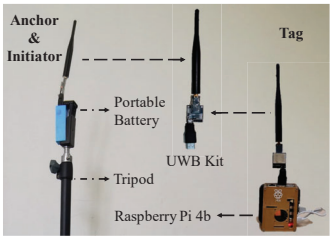

(a) Hardware of UWB devices.

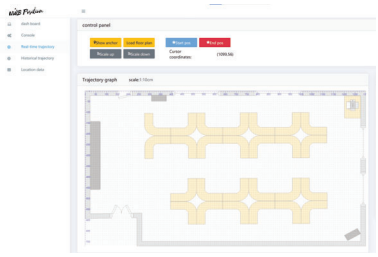

(b) UI for online localization system.

Fig. 9. Hardware platform and our online localization system.

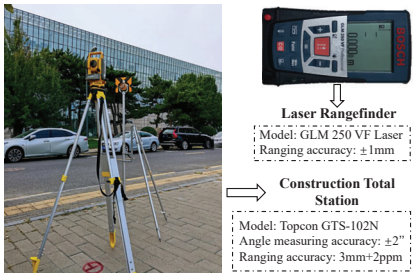

Fig. 10. Measuring instruments for ground-truth.

lower positioning accuracy than the TWR method. However, as inferred from the above analysis, VULoc can achieve a high positioning accuracy even compared to the TWR method and require no time synchronization.

4.2 Power Consumption Comparison

At first glance, VULoc may consume more power than the DS-TWR method as it requires more receptions, and packet reception causes more power than transmitting in UWB. However, after careful examination, we find that VULoc can consume less power than the DS-TWR method. According to the Decawave DW1000 datasheet [2] and Decawave user manual [4], the power consumed by a single packet is typically 31 μJ for transmissions and 56 μJ for receptions [69]. Given N anchors [1], a tag in VULoc may receive a total $(N+1)$ packets (Fig. 6) while the tag in DS-TWR would transmit 2 packets and receive N packets. As a result, the power consumption of VULoc can be calculated as $(N+1) \times 56\mu J$, and the power consumption of DS-TWR can be calculated as $(N \times 56 + 2 \times 31)\mu J$. For a typical scenario with $N = 4$, the power consumption of VULoc is 280 μJ, which is even slightly smaller than that of the DS-TWR, i.e., 286 μJ. Meanwhile, VULoc can conduct more reasonable power management due to two-fold:

- All tags can require positioning on demand because of the passive reception mode in VULoc, while the DS-TWR method requires careful scheduling design that brings additional power consumptions, e.g., conflict avoidance and dynamic topology changes.
- VULoc can also save much more power when there are large amounts of tags positioning simultaneously since it can significantly reduce collisions. DS-TWR method requires much more retransmissions due to collisions to achieve satisfactory performance and causes much more power overhead.

However, it is noteworthy that the energy of pure UWB systems is inefficient in the face of mobile tags since tag discovery can consume lots of energy due to the unbalanced energy budget between the transmission and reception of packets in UWB. For example, the UWB radio can consume 24× more power than the BLE radio in the period of listening [17]. It inspires us that we can integrate our solution with low power techniques, e.g., BLE, to design a wiser and more efficient positioning solution in the future.

5 IMPLEMENTATION

5.1 Hardware Platform

As shown in Fig. 9a, we implement VULoc on UWB devices with the commercial DW1000 chip, an STM32F103T8 MCU, and a five dBi antenna. The node uses an LNA on the Rx path to improve ranges as described in APS004 [3].

[1]Note that the initiator is also a special anchor

The DW1000 is configured to use channel 2 (a bandwidth of 499.2 MHz and a carrier frequency of 3993.6 MHz), a data rate of 110 kbps, and the pulse repetition frequency (PRF) of 16 MHz.

There are three different roles in VULoc, i.e., the *initiator*, the anchor, and the tag. They are all based on the same hardware platform. In our experiments, the *initiator* along with other anchors are installed on tripods so that we can move them to different positions, as shown in the left part of Fig. 9a. A portable battery is attached to each device for power supply. At present, we connect the tag to a Raspberry Pi 4b through USB, as shown in the right part of Fig. 9a. The Raspberry Pi is used for out-of-band control, including collecting data, dealing with the timestamps, and transmitting data to the server through TCP/IP.

5.2 Software Implementation

For brevity, we introduce the basic algorithm implementation. We adopt the Chan algorithm to calculate a candidate position based on distance difference estimations. We treat the Chan algorithm's output as a coarse result and use it as the start location for the non-linear least squares solver to reduce the overhead. We use the Levenberg-Marquardt algorithm [50] [53] for the non-linear least squares solver.

Furthermore, we develop an online localization system based on the design of VULoc. To ensure prompt and efficient processing, the whole system is divided into two layers, i.e., the edge layer and the cloud layer. At the edge layer, we connect each tag to a Raspberry Pi 4b. The Raspberry Pi has a 4-core 64-bit Cortex-A72 processor and 2GB RAM. It is responsible for streaming the data to the cloud. We also implement a Python program on the Raspberry Pi to continuously read the data from the UWB device through USB and extract the required timestamps. Then, the Raspberry Pi estimates the final position based on the timestamps and our localization method. Finally, the Raspberry Pi uploads the result into the cloud database. To visualize the result, we develop a website to show real-time position information based on data from the database. As shown in Fig. 9b, the website also supports rich functions, such as uploading the floor plans, storing and reshowing historical data, map zoom in/out, etc.

6 EVALUATION

6.1 Methodology

We first evaluate the localization error of VULoc in terms of different indoor environments. For each environment hereinafter, we use a total of five anchors with the anchor A_0 as the first *initiator*.

i) Hall. We set up VULoc in a hall as shown in Fig. 11a. The size of the hall is about $10\,m \times 6\,m$ with almost no obstacles.

ii) Classroom. As shown in Fig. 11b, the size of the room is about $12\,m \times 8\,m$. There are many reflectors and obstacles in the room, such as tables and chairs.

iii) Laboratory. This lab is about $12\,m \times 7\,m$ as shown in Fig. 11c. The lab contains many tables, chairs, and computers. Furthermore, people walk around the lab frequently during the experiment.

We then investigate the scalability of VULoc by locating 30 tags simultaneously and show the performance in terms of a different number of tags. Meanwhile, we compare VULoc with the state-of-the-arts:

- DS-TWR [34]: the widely used two-way ranging method for accurate UWB-based localization.
- ATLAS [62]: an open-source TDOA-based UWB localization method. A reference tag is required to synchronize the time between anchors.

In the next experiment, we choose an outdoor parking lot of $80\,m \times 90\,m = 7200\,m^2$ to compare the performance of VULoc in areas of different sizes. Specifically, we choose a small area of $10\,m \times 8\,m = 80\,m^2$ and a large area of $80\,m \times 90\,m = 7200\,m^2$ for evaluation, as shown in Fig. 15a and 15b.

We finally show the tracking performance of VULoc in three indoor environments and demonstrate the efficiency of the anchor scheduling algorithm in NLOS settings.

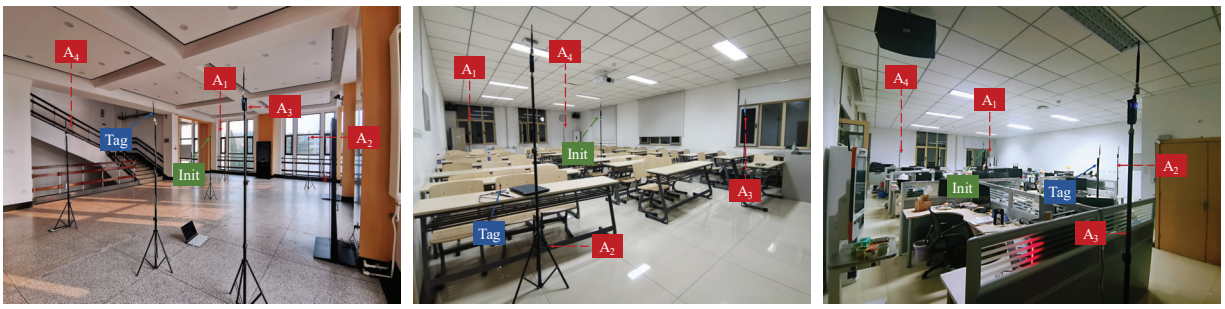

(a) The hall. (b) The classroom. (c) The laboratory.

Fig. 11. Various indoor environments for evaluation.

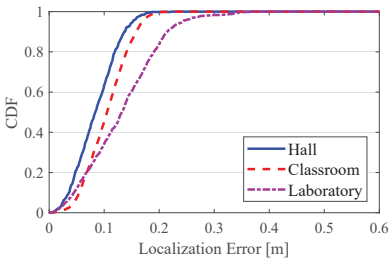

Fig. 12. VULoc in different environments.

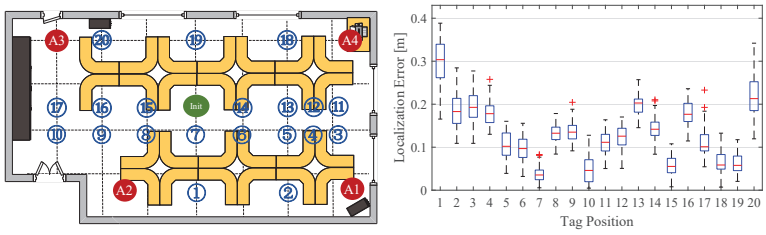

(a) The indoor floor map. (b) Localization error of 20 positions.

Fig. 13. Localization in the laboratory.

6.1.1 UWB Configuration. We set UWB devices to work in channel 2 with a central frequency of 3993.6 MHz, a bandwidth of 499.2 MHz, a data rate of 110 kbps, and a PRF of 16 MHz. The *initiator* sends a *Poll* message every 50 ms in VULoc. A ranging process (see Fig. 6) lasts about 20 ms for position measurement.

6.1.2 Ground-truth. As shown in Fig. 10, we leverage two measuring instruments for ground-truth measurement. We adopt the GLM 250 VF laser to measure the distance and position for short-range measurement and indoor environments. The ranging error of the device is under 1 mm. For long-range measurement and outdoor environments, we use the Topcon GTS-102N construction total station shown in the left part of Fig. 10 for ground-truth measurement. The device is widely used in building construction, surveying, and mapping. The device's position error is 3 mm, and the angle error is 2″.

6.2 Localization Performance in Different Indoor Environments

As shown in Fig.11, we choose three environments, i.e., the hall, the classroom, and the laboratory for indoor evaluation. We divide each space into grids and collect data from at least 10 different points on the grids. For each point, we collect data three times, and each time lasts for about 30 seconds.

6.2.1 Overall Performance. Fig. 12 shows the CDF of localization error under three different environments. We see that the median localization error is 8.4 cm in the hall, 10.5 cm in the classroom, and 13.2 cm in the laboratory. The localization accuracy in the hall is higher than those in the other two environments. The accuracy in the

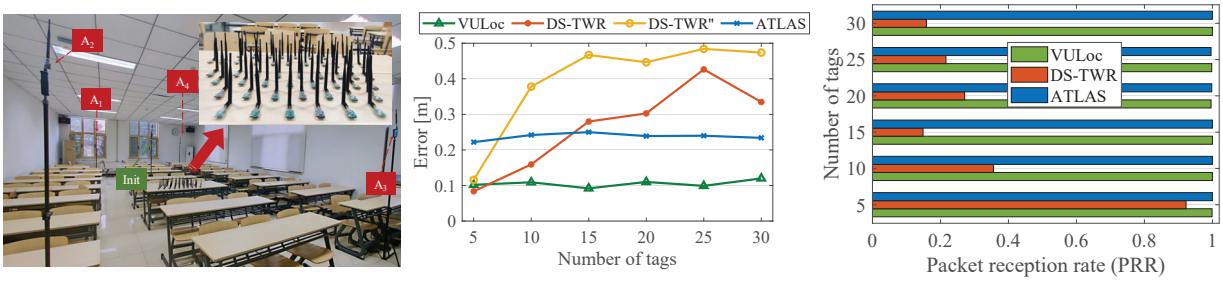

(a) Large-scale deployment of 30 tags.

(b) Positioning accuracy.

(c) Packet reception rate (PRR).

Fig. 14. Comparison of different methods with 30 tags deployment in the classroom.

laboratory is the lowest among those three environments. This is because the laboratory environment is more complicated than the other two environments. There are more crowded furniture and people in the laboratory, posing more obstacles and multi-path effects. The result shows that VULoc can adapt to different environments and achieve centimeter-level localization results.

6.2.2 Detailed Performance in the Laboratory. In order to better illustrate the indoor localization performance, we show a detailed evaluation of VULoc in the laboratory environment with crowded reflectors. We divide the space into grids and choose 20 different tag positions in the laboratory, as shown in Fig. 13a. As we can see, these positions are marked with circled IDs. The four anchors are marked as red circles, while the initiator is marked as a green circle. Fig. 13b shows the error distribution. We can see that the localization error is below 20 cm for most points. There are two tags with errors slightly higher than 30 cm. We then carefully examine these points with large errors. We find that those points are around the border (e.g., positions 1 and 20) of the entire area and thus tend to have larger errors. We think it may be due to the poor convergence of the positioning algorithm on the boundary points. We thus can expand the anchors' coverage area or deploy more anchors to reduce localization errors in practice.

6.3 Localization Performance with Large-scale Deployment

In this experiment, we investigate the scalability of VULoc with 30 tags. At the same time, we compare its performance with two novel methods, i.e., the DS-TWR method and an open-source TDOA method (ATLAS [62]).

In DS-TWR, the tag works with two round-trip exchanges to measure the distance to each anchor. With the measured distance, we run a sphere intersection algorithm to calculate the position. In ATLAS, we leverage a reference tag to transmit sync data and measure TDOA information for the target. Then, we adopt the TDOA algorithm used by VULoc to calculate the localization result. Note we use the same parameter for range calibration for all three methods in order to fairly compare the localization algorithm.

We compare their performance with a different number of tags working simultaneously in the classroom, as shown in Fig 14a. For ease of data collection, tags are connected to a USB hub and then are connected to processing computers through USB. For VULoc and ATLAS, there is no need to design scheduling protocols since tags in those two methods are passively listening. For DS-TWR, we adopt a pure ALOHA protocol and add a random delay of 300 ms for tags to avoid collisions. We run the experiment for 5 minutes for each method adopted.

Fig. 14b shows the localization error with a different number of tags. Fig. 14c shows the packet reception rate (PRR) of different methods. We see that VULoc and ATLAS achieve a localization error of 10.2 cm and 24.1

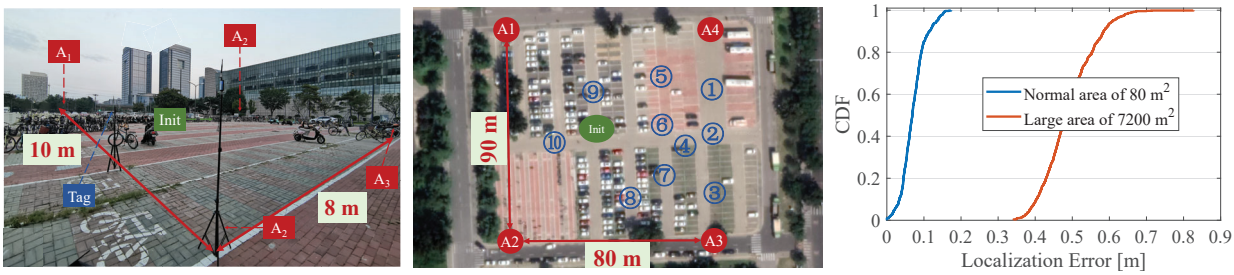

(a) Deployment in the parking area. (b) Bird view of the area. (c) Localization error.

Fig. 15. Performance of VULoc in normal area and large area.

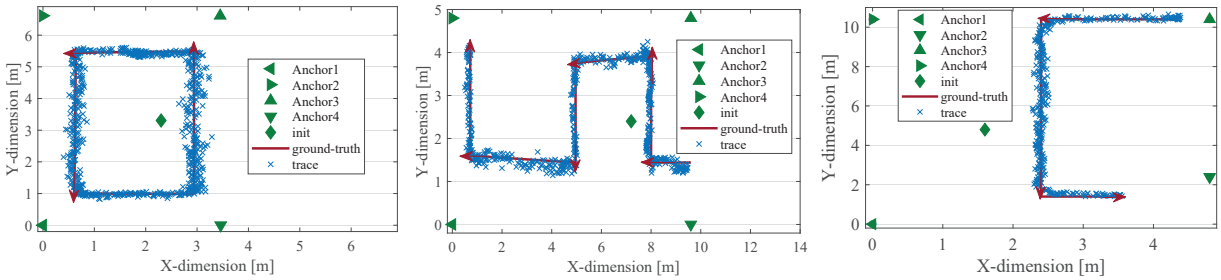

(a) Tracking in the hall. (b) Tracking in the classroom. (c) Tracking in the laboratory.

Fig. 16. Tracking with VULoc. The blue dots are the localization results and the redline is the ground-truth.

cm, respectively, regardless of the number of tags. On the contrary, the localization error of DS-TWR increases significantly with the increased number of tags. We can see that there are many incorrect timestamps with large errors for DS-TWR due to severe packet collisions, which further leads to large localization errors. The PRR of VULoc and ATLAS keep nearly 100% due to passive reception mode, while the PRR of the DS-TWR method drops significantly when the number of tags ≥ 10. As the localization cannot be calculated for a collided packet, we assume the positioning error of collided packets as 0.5 m and re-calculate the error of DS-TWR as DS-TWR″. We also plot the result of DS-TWR″ in Fig. 14b. We can see that the error of DS-TWR″ is closer to 0.5 m with the increasing number of tags due to the increased number of collided packets.

We see that VULoc achieves about 57.6% less localization error than ATLAS even without any synchronization. DS-TWR will achieve slightly better accuracy than our work when the number of tags is very small. However, DS-TWR degrades quickly when the number of tags increases. As a result, VULoc reduces 69.6% errors on average compared to DS-TWR. To conclude, VULoc maintains satisfactory performance in large-scale deployment, which is very important in actual applications. The other two methods cannot achieve high accuracy and scalability simultaneously.

6.4 Localization Performance in Different Areas.

For practical applications, the coverage of the positioning system is also essential. For this reason, we explore the performance of VULoc in different sizes of deployment areas. We evaluate VULoc in an outdoor parking lot with an area of 7200 m^2. For comprehensive assessments, we conduct experiments in the following two scenarios.

i) A normal area of the parking lot. First, we choose a part of the parking lot as shown in Fig. 15a. The area is about $10\,m \times 8\,m$, which is close to the normal size of most indoor rooms. The initiator and anchors are marked in the figure as well.

ii) A large area of the parking lot. To evaluate the performance of VULoc in a large area, we thus choose the entire parking lot, whose size is about $80\,m \times 90\,m$. Fig. 15b shows the satellite map of the parking lot and the detailed deployment.

In each scenario, we randomly choose 10 positions for evaluation. As the area size becomes large, we leverage the Topcon GTS-102N construction total station to measure the ground truth. The result is shown in Fig. 15c.

We see that the median localization error of the normal area is 6.3 cm, while the median localization error of the large area is about 48 cm. The error becomes larger in the large area being two-fold. First, UWB devices incur a large time measurement error in wide areas. Second, we observe that the anchors in the large area are surrounded by trees and vehicles, which may block and reflect the UWB signal, resulting in an increase in error. However, we think such accuracy is still acceptable considering such a large area.

6.5 Tracking with VULoc

We finally investigate the performance of VULoc for tracking in three indoor environments shown in Fig. 11. We ask volunteers to hold the tag and move along the predefined traces at their usual walking speed.

The tracking result is shown in Fig. 16. The green marks show the positions of anchors. The red line shows the ground truth with arrows indicating the moving direction. The blue dots show the tracking result. Note that those tracking points are raw results with no filtering and other data processing method.

We can see from the results that the tracking points are close to the actual trajectory in all three environments. It indicates that VULoc can achieve a good performance in tracking. We also observe some offset between the practical trajectory and the actual one, especially at the turning point. We think the noise may be introduced by volunteers as it is not easy to follow the predefined trajectory holding the UWB device just in hands at the turning points. It is not easy for people to follow a predefined long straight line since the tracked points deviate more from the actual path, especially for a long tracking distance (e.g., vertical lines in Fig. 16a). We also see that the tracked points can be dense or sparse as the speed of persons' movement varies.

We finally summarize the median and 90% tracking error in these environments in Tab. 17. The result is slightly larger than that of static points shown in Fig. 12 due to unavoidable human mistakes as discussed above. However, we think such results are enough to demonstrate the feasibility and effectiveness of our method.

6.6 Evaluation of Anchor Scheduling Algorithm

We now show the NLOS elimination effects by our anchor scheduling algorithm. As VULoc involves both anchor links and tag links for localization, we let volunteers block both links separately and evaluate the performance of the anchor scheduling algorithm. Specifically, we first examine the performance under static blocks by blocking anchor and tag link #1 or #2. Then we let the volunteer move around to build a dynamic NLOS environment. We finally demonstrate the performance of VULoc under two blocked links.

The result is shown in Fig. 18. Without any link blockages, the localization error is very small, i.e., about 0.12 m. When one link is blocked, the localization error increases significantly no matter of static or dynamic blocks without the anchor scheduling algorithm. This is because such a blocked link can lead to large ranging errors and further lead to large localization errors. Meanwhile, we see that the increase of error is unpredictable and

Environments	Median Error (m)	90% Error (m)
Hall	0.117	0.185
Classroom	0.142	0.214
Laboratory	0.155	0.236

Fig. 17. Tracking errors

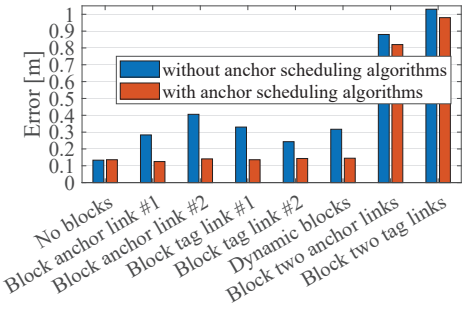

Fig. 18. Performance of anchor scheduling algorithm under different blocked links.

varies with different blocked links, e.g., about 0.28 m when blocking anchor link #1 and about 0.41 m when blocking anchor link #2. With the anchor scheduling algorithm, we can achieve a stable and highly-accurate result comparable to the case without blocks since we can choose the best-link anchors for localization by the algorithm.

When two links are blocked, the localization error increases rapidly, even with the anchor scheduling algorithm. The scheduling algorithm is based on link estimation and anchor selection. When two links are blocked, the remaining links are not enough to achieve accurate localization. Thus, our work also fails to work when most of the anchors are blocked. Nevertheless, the anchor scheduling algorithm can always find the best links for localization, thus achieving a better result than that without the algorithm.

7 DISCUSSION

Through extensive evaluations, we show the performance of VULoc in a wide area of $7200m^2$, a large-scale deployment with 30 nodes and various indoor environments across static positions and mobile trajectories. The results, along with the theoretical analysis (Sec. 4.1), show that VULoc can achieve a very high positioning accuracy and support a large number of targets without synchronization overhead. However, there are some issues that we need to discuss in detail and clarity.

The influence of the target's speed. The basic principle of VULoc assumes that the range between the target and the *initiator* should keep constant in one measurement. Therefore, when the target moves very fast, the positioning result of VULoc may be significantly affected. It is a common issue for localization techniques and systems that combine multiple anchors for localization, like the TDOA method. We thus left it for future work. Nevertheless, we think VULoc can meet most applications with a moderate speed localization target. For instance, suppose that the system can tolerate 10 cm displacements of the target during one measurement (20 ms), VULoc thus can satisfy applications with a speed of $\frac{10\times10^{-2}}{20\times10^{-3}} \times \frac{3600}{10^3} = 18\,km/h$.

None-line-of-sight (NLOS) problem. Though UWB is resistant to multi-path thanks to its high bandwidth, its performance may degrade significantly in NLOS environments [16, 44, 68]. We also verify the problem in our preliminary study. To address the problem, we design an anchor scheduling algorithm that lets each anchor takes turns to be the *initiator* and adopt two metrics inferred from the channel to judge the quality of receptions. However, such a method can only select three estimates with the best reception quality and fails to work when most anchors are affected by NLOS. There is a large amount of work that identifies and mitigates the NLOS effect [12, 19, 24, 35, 47, 51] in the literature. We can leverage those designs to minimize the NLOS effect in the future for actual applications.

Table 1. Comparison of UWB localization techniques.

Localization Technique	Representative Work	Accuracy	Scalability	Update rate	Calibration Overhead	Synchronization
Two-way Ranging (TWR)	[33] [10] [42] [41]	★★★★★	★★★	★★★	High	Not required
Time Difference of Arrival (TDOA)	[43] [63] [48]	★★★	★★★★★	★★★★	High	Required
Angle of Arrival (AoA)	[69] [67] [26]	★★	★★★★	★★★★	High	Not required
Concurrent TDOA	[31] [23] [22]	★★★	★★★★★	★★★★★	High	Required
Concurrent AoA	[37]	★★	★★★★★	★★★★★	High	Required
Virtual-TWR (V-TWR)	VULoc	★★★★	★★★★★	★★★★	Low	Not required

The general validity of our V-TWR method. In this paper, we implement the idea and system in DW1000, one of the most widely used UWB transceivers available off-the-shelf today. Nevertheless, the fundamental concept of the V-TWR method can also be used in other timestamp-based ranging techniques, e.g., WiFi FTM protocol [40, 58]. We believe VULoc can bring gains and benefits to those ranging and positioning techniques.

8 RELATED WORKS

We summarize the current localization techniques for UWB in Tab. 1. As we see from the table, we divide the state-of-art UWB localization techniques into four categories, namely Two-way Ranging (TWR), Time Different of Arrival (TDOA), Angle of Arrival (AoA), and the recent concurrent UWB localization techniques including concurrent TDOA and concurrent AoA. We compare those techniques from five aspects, i.e., accuracy, scalability, the update rate of positions, calibration overhead, and the requirement for time synchronization.

Two-way Ranging (TWR). Most existing UWB based localization systems adopt the TWR method, which requires multi-packet exchange between two UWB devices for ranging, as the method provides a high positioning accuracy without time synchronization [11, 18, 27, 28, 33, 36, 41, 45, 46, 59, 70]. The two widely used TWR methods are single-sided two-way ranging (SS-TWR) and double-sided two-way ranging (DS-TWR), as recommended by the IEEE 802.15.4 standard [34]. The SS-TWR method requires one trip of request-reply exchange between two devices to calculate their range, while the DS-TWR method adds one more transmission based on the SS-TWR to increase the ranging accuracy, yet causing message and delay overhead. SurePoint [41] further improves the ranging accuracy by exploiting the channel diversity and requires 30 packet exchanges for one measurement. Intuitively, the more data are exchanged, the more accurate the positioning results tend to be. Nevertheless, those approaches requiring multiple-message exchange between the devices may incur a high communication overhead and hinder the system's scale. As the number of UWB devices increases, the possibility of packet conflict also greatly increases, making it hard to locate many devices and thus causing poor scalability for localization targets. Otherwise, it will significantly increase the latency to estimate a single location. The update rate of the TWR method may also be undesirable due to poor scalability.

Time Difference of Arrival (TDOA). The TDOA-based UWB localization systems [43, 48, 60, 62, 63] determine the position of a tag by the time difference of arrival (TDOA) between anchors. The tag only needs to passively receive packets from anchors. The scalability and the update rate of the method are very high. However, due to the asynchrony of the device clock, those TDOA-based UWB localization systems require a tight time synchronization to achieve satisfactory positioning accuracy. For instance, Harmonium [43] achieves time synchronization via wired technology to maintain good performance. The clock synchronization problem is

still an open issue, and there is no perfect solution. Thus, the positioning accuracy of TDOA is usually lower than that of the TWR method. We also show that the clock drift of devices can also cause a significant error in the TDOA method, as discussed in Sec. 4.1.

Angle of Arrival (AoA). There are works [15, 29, 39, 49, 57] that try to measure the AoA of two UWB devices and use it for localization. Yet, most those approaches are limited to simulations [29, 39, 49]. Recently, some commercially available UWB-kits [8, 26] which can support AoA estimation have emerged. [26] proposes to use the phase difference of arrival (PDOA) to test the AoA estimation of the DW1000 [2] kit, while ULoc [69] further advances the technology by offering a 3D AoA estimation. Since the AoA estimation requires only one packet from the target and needs no time synchronization, it can provide high scalability and high update rates for localization. However, the positioning accuracy of the AoA technique is far from satisfactory for two reasons. First, the AoA resolution is highly limited by the antennas' number, size, and craftsmanship. Second, even a tiny angle deviation can cause a significant error, especially for a long range. For instance, assuming the target is in the 45° direction of the anchor, a deviation of 3° can leads to an error of $1.106\,m$ at a distance of 10 meters $(10 \times \tan(45^\circ + 3^\circ) - 10 \times \tan(45^\circ))$. As a result, the AoA technique is usually combined with other localization techniques for robust applications.

Concurrent techniques. There have been recent advances in concurrent techniques [21–23, 31, 32, 37, 38, 65]. Concurrent ranging [21, 38] is built on the TDOA method but significantly shortens the time interval of packets between anchors, and thus significantly reduces the delay of localization. Typically, concurrent ranging systems exploit synchronous transmissions to perform ranging and extract TDOA information through the channel impulse response (CIR) of the concurrent received messages by the tag. For example, Chorus [23] and SnapLoc [31] present a GPS-like passive localization scheme based on concurrent ranging that supports a limitless number of tags. Recently, Anguloc[37] proposes a concurrent-AoA scheme that estimates the AoA of concurrent packets through the CIR. Therefore, concurrent techniques can offer a very fast update rate and high scalability of localization targets. Yet, as we see, it comes at the expense of packet reception rate (PRR) since only one packet may be received in one measurement. Besides, it requires a tight time synchronization for anchors and accurate scheduling transmissions need to be designed for concurrent ranging.

In summary, as shown in Tab 1, the TWR method is superior in accuracy yet is inferior in scalability; the TDOA method achieves extensive scalability yet an inferior accuracy requiring tight time synchronization among anchors; the AoA method can provide the angle information and is usually combined with other techniques to achieve better results; the concurrent techniques reduce the positioning delay significantly yet at the expense of packet reception rate and require a tight time synchronization and accurate scheduling. In contrast with those existing UWB localization techniques, VULoc is one of its kind to achieve both high accuracy and large scalability with no synchronization overhead. Furthermore, to the best of our knowledge, VULoc is the first work that proposes to leverage the anchor ranging for auto-calibration while incurring no data exchange overhead.

9 CONCLUSION AND FUTURE WORK

Though the UWB technology is a promising technique to achieve accurate localization, we find existing works are hard to provide high accuracy for a large number of targets due to tedious synchronization and labor-intensive calibration overhead. We thus present VULoc, a UWB-based localization system that simultaneously achieves high accuracy and scalability with no synchronization and low calibration overhead. We implement VULoc on commercial DW1000 hardware, and extensive experiments show that VULoc can achieve accurate localization with a median error of 10.5 cm and 90% error of 15.7 cm, reducing the error of ATLAS (an open-source TDOA-based work) by 57.6% while supporting an unlimited number of tags with no synchronization and no manual calibration overhead.

We think VULoc can be a solid step towards UWB localization for the ubiquitous Internet of Things. Yet, there are many future works to improve VULoc's performance. First of all, though VULoc is capable of achieving high accuracy and supporting unlimited tags, its energy consumption is still a concern compared to other low power techniques. We can integrate our solution with low power techniques to design. For example, we can adopt a low power consumption approach similar to [17] for our approach. Second, VULoc designs an anchor scheduling algorithm and estimates link status to choose anchors to minimize the NLOS effect. However, such a method fails to work in severe NLOS environments, e.g., most anchors are blocked. We can adopt effective NLOS mitigation techniques to further increase system robustness. Last but not least, the auto-calibration method in our solution can also be improved, and the accuracy of UWB can further be enhanced. Yet, as we point out, the goal can only be achieved through tedious calibration operations at present [1, 55]. We think the advance in machine learning can give new inspirations to address this problem.

ACKNOWLEDGMENTS

This work is in part supported by NSFC No. 62172250, No. 61932013, Tsinghua University Initiative Scientific Research Program. Jiliang Wang is the corresponding author.

REFERENCES

[1] 2014. APS011 APPLICATION NOTE. https://www.decawave.com/wp-content/uploads/2018/10/APS011_Sources-of-Error-in-Two-Way-Ranging-Schemes_v1.1.pdf/.
[2] 2015. DW1000 datasheet. https://www.decawave.com/sites/default/files/resources/dw1000-datasheet-v2.09.pdf.
[3] 2018. APS004 APPLICATION NOTE. https://www.decawave.com/wp-content/uploads/2018/10/APS004_Increasing-the-Range-of-DW1000-Using-LNA_v1.6.pdf/.
[4] 2019. DW1000 user manual. https://www.decawave.com/wp-content/uploads/2019/07/DW1000-User-Manual-1.pdf.
[5] 2020. Dimension4 UWB RTLS. https://ubisense.com/dimension4/.
[6] 2020. Humatics Rail Navigation System. https://timedomain.com/products/humatics-rail-navigation-system/.
[7] 2020. UWB SOLUTIONS COMPATIBLE WITH APPLE'S U1 CHIP. https://www.qorvo.com/innovation/ultra-wideband/products/uwb-solutions-compatible-with-apple-u1/.
[8] 2021. NXP Ultra-wideband kit. https://www.nxp.com/products/wireless/secure-ultra-wideband-uwb/trimension-uwb-developmentkit:MK-UWB-DEV-KIT/.
[9] R. W. Schafer A. V. Oppenheim and J. R. Buck. 1989. Discrete-time signal processing. *Prentice-hall Englewood Cliffs* (1989).
[10] Amr Alanwar, Henrique Ferraz, Kevin Hsieh, Rohit Thazhath, Paul Martin, João Hespanha, and Mani Srivastava. 2017. D-SLATS: Distributed simultaneous localization and time synchronization. In *Proceedings of ACM Mobihoc*.
[11] Abdulrahman Alarifi, AbdulMalik Al-Salman, Mansour Alsaleh, Ahmad Alnafessah, Suheer Al-Hadhrami, Mai A Al-Ammar, and Hend S Al-Khalifa. 2016. Ultra wideband indoor positioning technologies: Analysis and recent advances. *Sensors* (2016).
[12] Abbas Albaidhani, Antoni Morell, and Jose Lopez Vicario. 2016. Ranging in UWB using commercial radio modules: Experimental validation and NLOS mitigation. In *Proceedings of IEEE IPIN*.
[13] Alireza Ansaripour, Milad Heydariaan, Omprakash Gnawali, and Kyungki Kim. 2020. ViPER: Vehicle pose estimation using ultra-wideband radios. In *Proceedings of IEEE DCOSS*.
[14] Apple UWB 2019. Apple built UWB into the iPhone 11. Here's what you need to know. https://www.cnet.com/news/apple-built-uwb-into-the-iphone-11-heres-what-you-need-to-know-faq/.
[15] G Dickey Arndt, Phong H Ngo, Chau T Phan, Julia Gross, Jianjun Ni, and John Dusl. 2010. *Ultra-Wideband Angle-of-Arrival Tracking Systems*. Technical Report.
[16] Valentín Barral, Carlos J Escudero, José A García-Naya, and Roberto Maneiro-Catoira. 2019. NLOS identification and mitigation using low-cost UWB devices. *Sensors* (2019).
[17] Andreas Biri, Neal Jackson, Lothar Thiele, Pat Pannuto, and Prabal Dutta. 2020. SociTrack: infrastructure-free interaction tracking through mobile sensor networks. In *Proceedings of ACM MobiCom*.
[18] Francisco Bonnin-Pascual and Alberto Ortiz. 2019. An UWB-based System for Localization inside Merchant Vessels. In *Proceedings of IEEE ETFA*.
[19] Roberto Casas, A Marco, JJ Guerrero, and J Falco. 2006. Robust estimator for non-line-of-sight error mitigation in indoor localization. *EURASIP Journal on Advances in Signal Processing* (2006).
[20] Yiu-Tong Chan and KC Ho. 1994. A simple and efficient estimator for hyperbolic location. *IEEE Transactions on signal processing* (1994).

[21] Pablo Corbalán and Gian Pietro Picco. 2018. Concurrent Ranging in Ultra-wideband Radios: Experimental Evidence, Challenges, and Opportunities. In *Proceedings of EWSN*.
[22] Pablo Corbalán and Gian Pietro Picco. 2020. Ultra-wideband concurrent ranging. *ACM TOSN* (2020).
[23] Pablo Corbalán, Gian Pietro Picco, and Sameera Palipana. 2019. Chorus: UWB concurrent transmissions for GPS-like passive localization of countless targets. In *Proceedings of IEEE IPSN*.
[24] Danilo Demarchi, Paolo Motto Ros, and Alessio Serrani. 2019. No-Line-Of-Sight Identification and Mitigation in a Real Time Indoor Ultra-Wide Band Localization System. (2019).
[25] Ashutosh Dhekne, Ayon Chakraborty, Karthikeyan Sundaresan, and Sampath Rangarajan. 2019. Trackio: tracking first responders inside-out. In *Proceedings of USENIX NSDI*.
[26] Igor Dotlic, Andrew Connell, Hang Ma, Jeff Clancy, and Michael McLaughlin. 2017. Angle of arrival estimation using decawave DW1000 integrated circuits. In *Proceedings of IEEE WPNC*.
[27] Enrique García, Pablo Poudereux, Álvaro Hernández, Juan Jesús García, and Jesús Ureña. 2013. DS-UWB indoor positioning system implementation based on FPGAs. *Sensors and Actuators A: Physical* (2013).
[28] Enrique García, Pablo Poudereux, Álvaro Hernández, Jesús Ureña, and David Gualda. 2015. A robust UWB indoor positioning system for highly complex environments. In *Proceedings of IEEE ICIT*.
[29] Waldemar Gerok, Mohamed El-Hadidy, Sondos Alaa El Din, and Thomas Kaiser. 2010. Influence of the real UWB antennas on the AoA estimation based on the TDoA localization technique. In *Proceedings of IEEE MECAP*.
[30] Mahanth Gowda, Ashutosh Dhekne, Sheng Shen, Romit Roy Choudhury, Lei Yang, Suresh Golwalkar, and Alexander Essanian. 2017. Bringing IoT to sports analytics. In *Proceedings of USENIX NSDI*.
[31] Bernhard Groβwindhager, Michael Stocker, Michael Rath, Carlo Alberto Boano, and Kay Römer. 2019. SnapLoc: An ultra-fast UWB-based indoor localization system for an unlimited number of tags. In *Proceedings of IEEE IPSN*.
[32] Bernhard Großwindhager, Carlo Alberto Boano, Michael Rath, and Kay Römer. 2018. Concurrent ranging with ultra-wideband radios: From experimental evidence to a practical solution. In *Proceedings of IEEE ICDCS*.
[33] Bernhard Großwindhager, Michael Rath, Josef Kulmer, Mustafa S Bakr, Carlo Alberto Boano, Klaus Witrisal, and Kay Römer. 2018. SALMA: UWB-based single-anchor localization system using multipath assistance. In *Proceedings of ACM SenSys*.
[34] IEEE 802 Working Group et al. 2011. Ieee standard for local and metropolitan area networks—Part 15.4: Low-rate wireless personal area networks (lr-wpans). *IEEE Std* (2011).
[35] Fredrik Gustafsson. 2010. Particle filter theory and practice with positioning applications. *IEEE Aerospace and Electronic Systems Magazine* (2010).
[36] Ismail Guvenc, Chia-Chin Chong, and Fujio Watanabe. 2007. NLOS identification and mitigation for UWB localization systems. In *Proceedings of IEEE Wireless Communications and Networking Conference*.
[37] Milad Heydariaan, Hossein Dabirian, and Omprakash Gnawali. 2020. Anguloc: Concurrent angle of arrival estimation for indoor localization with uwb radios. In *Proceedings of IEEE DCOSS*.
[38] Milad Heydariaan, Hessam Mohammadmoradi, and Omprakash Gnawali. 2019. R3: Reflection resilient concurrent ranging with ultra-wideband radios. In *Proceedings of IEEE DCOSS*.
[39] Naohiko Iwakiri and Takehiko Kobayashi. 2008. Ultra-Wideband Time-of-Arrival and Angle-of-Arrival Estimation Using Transformation Between Frequency and Time Domain Signals. *J. Commun.* (2008).
[40] Kevin Jiokeng, Gentian Jakllari, Alain Tchana, and André-Luc Beylot. 2020. When FTM discovered MUSIC: accurate WiFi-based ranging in the presence of multipath. In *Proceedings of IEEE INFOCOM*.
[41] Benjamin Kempke, Pat Pannuto, Bradford Campbell, and Prabal Dutta. 2016. Surepoint: Exploiting ultra wideband flooding and diversity to provide robust, scalable, high-fidelity indoor localization. In *Proceedings of ACM Sensys*.
[42] Benjamin Kempke, Pat Pannuto, and Prabal Dutta. 2015. Polypoint: Guiding indoor quadrotors with ultra-wideband localization. In *Proceedings of Workshop on Hot Topics in Wireless*.
[43] Benjamin Kempke, Pat Pannuto, and Prabal Dutta. 2016. Harmonium: Asymmetric, bandstitched UWB for fast, accurate, and robust indoor localization. In *Proceedings of IEEE IPSN*.
[44] Jasurbek Khodjaev, Yongwan Park, and Aamir Saeed Malik. 2010. Survey of NLOS identification and error mitigation problems in UWB-based positioning algorithms for dense environments. *annals of telecommunications-annales des télécommunications* (2010).
[45] Sivanand Krishnan, Pankaj Sharma, Zhang Guoping, and Ong Hwee Woon. 2007. A UWB based localization system for indoor robot navigation. In *Proceedings of IEEE International Conference on Ultra-Wideband*.
[46] Michael Kuhn, Cemin Zhang, Brandon Merkl, Depeng Yang, Yazhou Wang, Mohamed Mahfouz, and Aly Fathy. 2008. High accuracy UWB localization in dense indoor environments. In *Proceedings of IEEE International Conference on Ultra-Wideband*.
[47] Bao Long Le, Kazi Ahmed, and Hiroyuki Tsuji. 2003. Mobile location estimator with NLOS mitigation using Kalman filtering. In *Proceedings of IEEE WCNC*.
[48] Anton Ledergerber, Michael Hamer, and Raffaello D'Andrea. 2015. A robot self-localization system using one-way ultra-wideband communication. In *Proceedings of IEEE IROS*.

[49] Yong Up Lee. 2011. Weighted-average based aoa parameter estimations for LR-UWB wireless positioning system. *IEICE transactions on communications* (2011).
[50] Kenneth Levenberg. 1944. A method for the solution of certain non-linear problems in least squares. *Quarterly of applied mathematics* (1944).
[51] Ze Li, Zengshan Tian, Mu Zhou, Zhenyuan Zhang, and Yue Jin. 2018. An accurate and robust environment sensing algorithm for enhancing indoor localization. In *Proceedings of IEEE INFOCOM*.
[52] Valerio Magnago, Pablo Corbalán, Gian Pietro Picco, Luigi Palopoli, and Daniele Fontanelli. 2019. Robot localization via odometry-assisted ultra-wideband ranging with stochastic guarantees. In *Proceedings of IEEE IROS*.
[53] Donald W Marquardt. 1963. An algorithm for least-squares estimation of nonlinear parameters. *Journal of the SIAM* (1963).
[54] Dries Neirynck, Eric Luk, and Michael McLaughlin. 2016. An alternative double-sided two-way ranging method. In *Proceedings of IEEE WPNC*.
[55] Decawave APS014 APPLICATION NOTE. 2019. Antenna delay calibration DW1000-Based products and systems, Version 1.2.
[56] Pat Pannuto, Benjamin Kempke, and Prabal Dutta. 2018. Slocalization: Sub-uW Ultra Wideband Backscatter Localization. In *Proceedings of IEEE IPSN*.
[57] Idnin Pasya, Naohiko Iwakiri, and Takehiko Kobayashi. 2014. Joint direction-of-departure and direction-of-arrival estimation in a UWB MIMO radar detecting targets with fluctuating radar cross sections. *International Journal of Antennas and Propagation* (2014).
[58] Alejandro Blanco Pizarro, Joan Palacios Beltrán, Marco Cominelli, Francesco Gringoli, and Joerg Widmer. 2021. Accurate ubiquitous localization with off-the-shelf IEEE 802.11 ac devices. In *Proceedings of ACM MobiSys*.
[59] Alwin Poulose, Žiga Emeršič, Odongo Steven Eyobu, and Dong Seog Han. 2020. An Accurate Indoor User Position Estimator For Multiple Anchor UWB Localization. In *Proceedings of IEEE ICTC*.
[60] Nathan C Rowe, Aly E Fathy, Michael J Kuhn, and Mohamed R Mahfouz. 2013. A UWB transmit-only based scheme for multi-tag support in a millimeter accuracy localization system. In *Proceedings of IEEE WiSNet*.
[61] Zhang Shaohui, Qi Yuhao, Zhai FangWen, Lu Hongbo, and Song Yixu. 2022. UWB positioning optimization method based on redundant distance screening. *Journal of Tsinghua University* (2022).
[62] Janis Tiemann, Fabian Eckermann, and Christian Wietfeld. 2016. Atlas-an open-source tdoa-based ultra-wideband localization system. In *Proceedings of IEEE IPIN*.
[63] Janis Tiemann, Yehya Elmasry, Lucas Koring, and Christian Wietfeld. 2019. ATLAS FaST: Fast and simple scheduled TDOA for reliable ultra-wideband localization. In *Proceedings of IEEE ICRA*.
[64] D. Tse and P. Viswanath. 2005. Fundamentals of wireless communication. *Cambridge university press* (2005).
[65] Davide Vecchia, Pablo Corbalán, Timofei Istomin, and Gian Pietro Picco. 2019. Playing with fire: Exploring concurrent transmissions in ultra-wideband radios. In *Proceedings of IEEE SECON*.
[66] Maximilian von Tschirschnitz, Marcel Wagner, Marc-Oliver Pahl, and Georg Carle. 2019. Clock error analysis of common time of flight based positioning methods. In *Proceedings of IEEE IPIN*.
[67] Tianyu Wang, Hanying Zhao, and Yuan Shen. 2020. An efficient single-anchor localization method using ultra-wide bandwidth systems. *Applied Sciences* (2020).
[68] Kegen Yu, Kai Wen, Yingbing Li, Shuai Zhang, and Kefei Zhang. 2018. A novel NLOS mitigation algorithm for UWB localization in harsh indoor environments. *IEEE Transactions on Vehicular Technology* (2018).
[69] Minghui Zhao, Tyler Chang, Aditya Arun, Roshan Ayyalasomayajula, Chi Zhang, and Dinesh Bharadia. 2021. ULoc: Low-Power, Scalable and cm-Accurate UWB-Tag Localization and Tracking for Indoor Applications. *Proceedings of ACM IMWUT* (2021).
[70] Lukasz Zwirello, Tom Schipper, Marlene Harter, and Thomas Zwick. 2012. UWB localization system for indoor applications: concept, realization and analysis. *Journal of Electrical and Computer Engineering* (2012).